Multiscale Hybrid CFD/DSMC Simulation of Rocket-Induced Atmospheric Waves for Ionospheric Disturbance Prediction

G. K. Tavva[1] and G. W. Bowden[2]

[1] BITS Pilani, Pilani Campus, India
gktavva@gmail.com
[2] UNSW Canberra, Australia
g.bowden@unsw.edu.au

Abstract. Rocket exhaust plumes at high altitude generate acoustic and gravity waves that propagate into the ionosphere as traveling ionospheric disturbances (TIDs). We previously developed a one-way-coupled, two-dimensional (2D) axisymmetric hybrid Computational Fluid Dynamics (CFD)/Direct Simulation Monte Carlo (DSMC) framework for a Falcon 9 FT second-stage plume, reproducing the bow shock, inner shock, mixing layer, and exhaust core [3]. However, the 2D axisymmetric framework could not represent the gravitationally stratified thermosphere or the resulting asymmetric wave propagation associated with TIDs. Here, we extend the framework to three dimensions by coupling the existing 2D CFD and DSMC solutions, through a purpose-built converter, to a large-scale, gravitationally stratified 3D DSMC domain initialized using the NRLMSIS 2.0 empirical atmosphere. A dual-resolution strategy, using a smaller low-F_{num} domain for near-field plume accuracy and a larger high-F_{num} domain for wave-propagation coverage, is applied at 160 km, and the high-F_{num} configuration is then applied at 180 km, along the Falcon 9 FT Iridium NEXT-4 second-stage trajectory. The resulting simulation matrix is presented, with 2D and 3D results for the 160 km case and 3D results for the 180 km case, demonstrating acoustic-dominated wave generation and pronounced upper/lower asymmetry due to atmospheric stratification. The framework provides a computational approach for investigating plume-generated disturbances and their propagation through the high-altitude atmosphere.

Keywords: DSMC · Hybrid CFD/DSMC · Rocket plume · Acoustic-gravity waves · Traveling ionospheric disturbances · Rarefied gas dynamics

1 Introduction

Launch vehicles are widely reported to produce ionospheric disturbances, including traveling ionospheric disturbances (TIDs) associated with shock acoustic waves and ionospheric depletions from exhaust chemistry [4, 8, 9]. These disturbances are of interest for launch detection, atmospheric diagnostics, space situational awareness, and ionospheric disturbance prediction.

Modeling the plume is challenging because it spans continuum, transitional, and rarefied flow regimes as it expands into the thermosphere; the local breakdown of the continuum assumption and the resulting domain split are discussed in detail in our prior 2D study [3]. There, we reported a one-way-coupled, 2D axisymmetric hybrid CFD/DSMC framework – CFD for the collisional inner plume, coupled to particle-based DSMC [1] at a constant collision-frequency surface for the transitional and rarefied outer plume – which reproduced the bow shock, inner shock, mixing layer, and exhaust core of a Falcon 9 FT second-stage plume [3]. Full details of the CFD setup, the DSMC Variable Soft Sphere (VSS) collision model [7], and the species/collision parameters used are given there and are not repeated here.

Being axisymmetric, that framework could not represent the stratified density and temperature of the thermosphere, nor gravity and buoyancy effects on the expanding plume, and so could not capture the directional spreading of wave energy or the asymmetric structure associated with observed TIDs. This paper extends the framework into three dimensions, coupling the existing 2D CFD and 2D DSMC stages to a new, large-scale 3D DSMC stage that resolves plume–atmosphere interaction and acoustic-gravity wave generation self-consistently within a gravitationally stratified thermosphere (Sect. 2). We apply the extended framework to two trajectory points of the Falcon 9 FT Iridium NEXT-4 launch (Sect. 3), and present 2D and 3D results for the first of these, at 160 km altitude (Sects. 4–5). Section 6 describes results for the 180 km case followed by the conclusion that talks about the benefits of this methodology and observations made across both cases.

2 Extended 3D Multiscale Framework

2.1 Study Overview

The extended framework retains the 2D CFD and 2D DSMC stages described above for the near- and mid-field plume (out to a 5 km axial boundary), and couples them, through a new 2D-to-3D converter, to a large-scale 3D DSMC stage that resolves the plume–atmosphere interaction and wave generation in a gravitationally stratified thermosphere (Fig. 1). The CFD stage is implemented in ANSYS Fluent and the DSMC stages in SPARTA [6]; the converter and post-processing scripts are implemented in MATLAB.

2.2 Governing Equations

The Boltzmann transport equation solved by the 3D DSMC stage is unchanged in form from the 2D case, but is now solved over a fully 3D, gravitationally stratified domain, with a body-force term for gravity, $\mathbf{g}$, that was previously neglected:

$$\frac{\partial f}{\partial t} + \mathbf{v} \cdot \nabla_{\mathbf{x}} f + \mathbf{g} \cdot \nabla_{\mathbf{v}} f = \left(\frac{\partial f}{\partial t} \right)_{\text{coll}} . \tag{1}$$

Collisions continue to be represented with the VSS model [7], now on a 3D adaptive Cartesian grid, using the same per-species parameters as in the prior 2D study [3]; F_{num} again denotes the ratio of real to simulated particles.

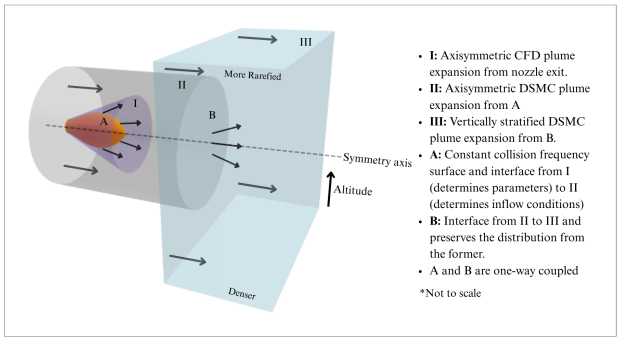


Fig. 1: Overall extended 3D multiscale simulation framework.

2.3 2D DSMC to 3D DSMC Converter

A converter maps the axisymmetric 2D DSMC solution onto a 3D Cartesian inlet for the 3D DSMC stage. It (i) extracts flow properties along the 5 km outlet boundary, (ii) interpolates the radial distributions with a Piecewise Cubic Hermite Interpolating Polynomial (PCHIP), (iii) maps the resulting axisymmetric field (n, T, $\mathbf{v}$, T_{rot}, T_{vib}, X_i) into 3D Cartesian space, reconstructing the transverse vertical and horizontal velocity components as $v_y = v_r\, y/r$, $v_z = v_r\, z/r$, with $r = \sqrt{y^2 + z^2}$; and (iv) applies atmospheric stratification beyond the inlet using the NRLMSIS 2.0 empirical model [5], giving a gravity-consistent, hydrostatic thermosphere profile with altitude-dependent number density, temperature, and composition (N_2, O_2, O). Together with the exhaust species carried over from the CFD/2D DSMC stages, the 3D DSMC study considers seven species in total: N_2, O_2, O, H_2O, CO_2, H_2, and CO.

2.4 Dual-Resolution 3D DSMC

A single 3D DSMC domain that is simultaneously large enough to capture the plume and its wave generation, and fine enough to resolve near-field shock structure, is demanding computationally. We therefore run two complementary 3D DSMC cases at 160 km (Table 1): a smaller domain with low F_{num} (Case 1) for near-field accuracy, and a larger domain with high F_{num} (Case 2) for wave-propagation coverage. Symmetry is assumed across the XY plane (gravity along $-Y$, plume axis along $+X$), extending the domain in both cases without additional computational effort.

Table 1: Comparison of the two 3D DSMC cases.

	Case 1: low F_{num}	**Case 2: high F_{num}**
Purpose	Resolve near-field detail	Resolve wave propagation
Accuracy	High, locally	Lower locally, domain-wide
Domain	X : 5–25 km, Y : ±15 km Z : 0–15 km	X : 5–45 km, Y : ±30 km Z : 0–30 km

3 Simulation Cases

The simulation conditions are based on the Falcon 9 FT Iridium NEXT-4 launch (22 December 2017), using the same trajectory, chamber conditions ($p_c = 10.8$ MPa, $T_c = 3670$ K), nozzle radius ($r_e = 1.4852$ m), and exhaust mole fractions ($x_{H_2O} = 0.3374$, $x_{CO_2} = 0.2885$, $x_{H_2} = 0.1558$, $x_{CO} = 0.2183$) as the prior 2D study [2, 3]. Two trajectory points are considered (Table 2), spanning different thermosphere conditions (from NRLMSIS 2.0) and rocket velocities; the CFD-supplied plume inflow is assumed identical across all cases.

Table 2: Simulation matrix: thermosphere/trajectory conditions.

Alt. (km)	N ($\times 10^{15}$ m^{-3})	T (K)	V_∞ (m/s)	N_2	O_2	O
160	22.98	649.1	2469.2	0.5627	0.0607	0.3766
180	9.89	703.9	2798.1	0.4791	0.0433	0.4776

4 2D CFD and 2D DSMC Results: 160 km Case

The 2D axisymmetric CFD solution for the 160 km case was previously reported by Bowden et al. [3]. The $\nu_{H_2} = 250$ Hz collision-frequency surface from the CFD solution defines the inflow boundary for the 2D DSMC stage, which captures the key features of the outer plume, including the bow shock, mixing layer, and inner shock surrounding the exhaust core. At 160 km, the relatively low relative kinetic energy of incoming thermospheric molecules results in a comparatively low bow-shock temperature. The resulting steady-state solution at the 5 km boundary is subsequently used as the inlet for the 2D-to-3D conversion and downstream 3D DSMC simulations.

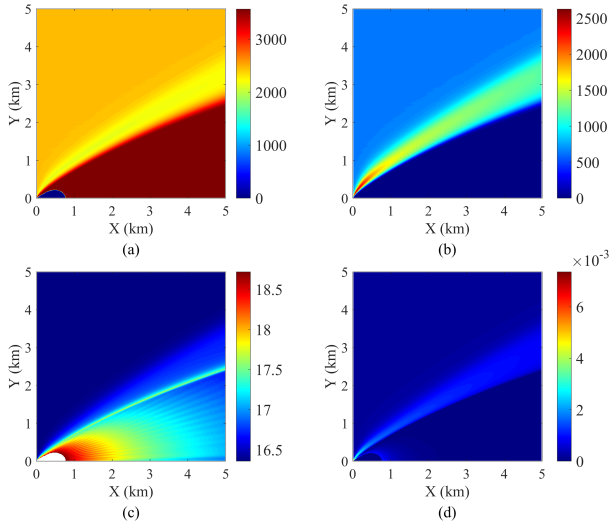


Fig. 2: 2D DSMC results for the 160 km case: (a) speed, (b) temperature, (c) number density ($\log_{10}(N\ [\mathrm{m}^{-3}])$), and (d) pressure.

5 3D DSMC Results: 160 km Case

5.1 Case 1: Low F_{num}, Small Domain

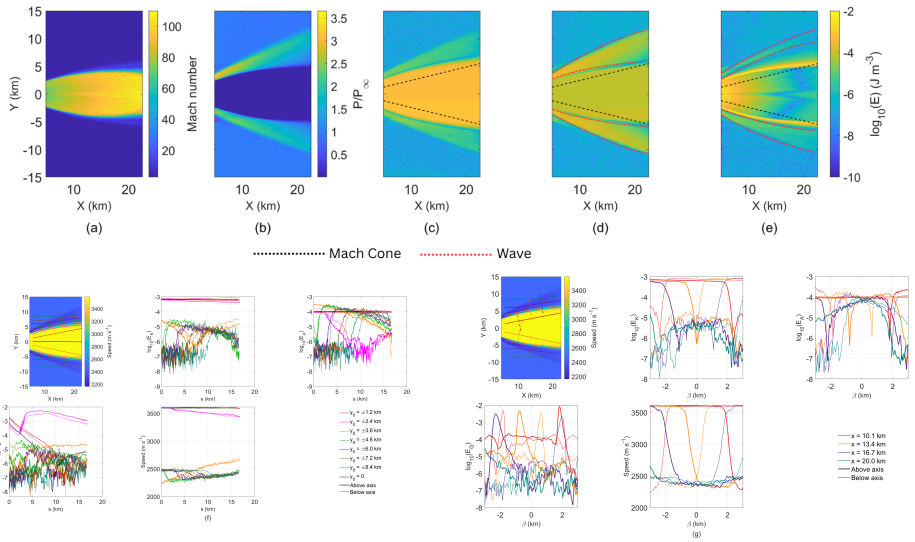


Fig. 3: 3D DSMC Case 1, 160 km case (XY Slice): (a) Mach number, (b) pressure ratio, (c) $\log_{10}(E_K)$, (d) $\log_{10}(E_A)$, and (e) $\log_{10}(E_G)$; (f) α along the streamline direction and (g) β perpendicular to the streamline direction.

Wave perturbations are decomposed into kinetic, elastic (acoustic), and thermobaric (gravity) potential energy densities, E_K, E_A, E_G, following the acoustic-gravity wave framework of Yeh and Liu [10].

A very high downstream Mach number is observed, driven by a sharp thermal drop. Variations above and below the plume axis reflect the thermospheric stratification, with a higher pressure ratio in the upper half. Disturbances are primarily acoustic rather than buoyant, based on E_A dominating over E_G through most of the domain; elevated thermobaric potential energy occurs over a markedly thicker region above the axis than below, indicating an asymmetric gravity-wave response. The kinetic, elastic, and thermobaric energy densities propagate at an angle slightly greater than the Mach angle to the axis. Along streamlines inside the inner shock, E_A stays roughly constant while E_G drops gradually; the extracted β-cuts (Fig. 3 (g)) are an effective diagnostic for the spatial position of the propagating waves.

5.2 Case 2: High F_{num}, Large Domain

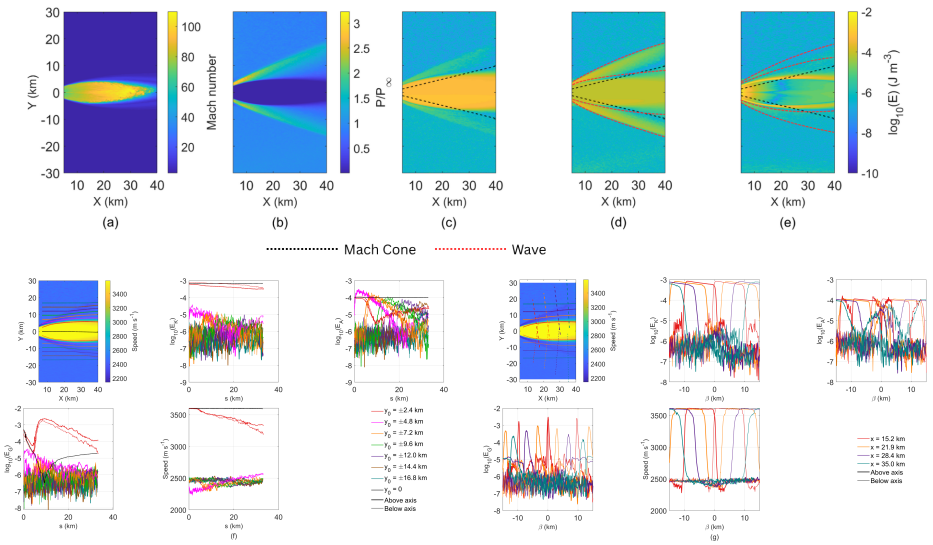


Fig. 4: 3D DSMC Case 2, 160 km case (XY Slice): (a) Mach number, (b) pressure ratio, (c) $\log_{10}(E_K)$, (d) $\log_{10}(E_A)$, and (e) $\log_{10}(E_G)$; (f) α along the streamline direction and (g) β perpendicular to the streamline direction.

At the larger domain scale, the bow shock continues to curve towards the Mach angle, and the Mach number peaks around $x = 30$ km before decreasing downstream as thermosphere inflow raises the local pressure. The inner plume region shows a distinct behavior from the external waves. The low-pressure core ($P/P_\infty \ll 1$) reaches a maximum radius of ≈ 4.7 km near $x \approx 20$–25 km and then narrows again to ≈ 3.8 km by $x = 40$ km. The dividing streamline, which separates exhaust gas from entrained thermospheric gas and effectively sets the shape of the body driving the external waves, converges far more slowly. Streamlines seeded at $y_0 = \pm 2.4$ km are still at $|y| \approx 6$ km at $x = 40$ km and have not yet turned back towards the axis (Fig. 4, bottom left). The plume therefore acts as a long, slender, open-ended body whose effective radius is considerably larger than that of its low-pressure core. Differences persist above and below the axis: shock amplitudes (absolute) are larger above than below, while shock strengths (relative) are lower above than below. The thermobaric potential energy stays largely localized around the mixing region rather than propagating outward as a gravity wave. A Mach disc is not clearly observed, either because the flow is highly rarefied at this scale or because the domain needs further extension.

Bow shock evolution, plume expansion, pressure/density perturbations, and acoustic/gravity wave structures are consistent across Cases 1 and 2. Increasing F_{num} and enlarging the domain therefore costs little accuracy for the quantities of interest here. The same shock and wave behavior is recovered, and the energy-density and streamline diagnostics follow the same trends, so the high-F_{num} case remains an acceptable way of measuring wave features. This is why only the high-

F_{num} configuration was run for the 180 km case (Sect. 6). It also suggests the approach can be extended to still larger domains, where the wave field is better resolved and wave-based launch detection becomes more practical.

6 3D DSMC Results: 180 km Case

This case represents a further point along the same Falcon 9 FT Iridium NEXT-4 trajectory. The CFD-supplied plume inflow is assumed identical at both altitudes, but the 2D DSMC stage is re-run for each using the corresponding ambient conditions (Table 2). Below are the plots for 180 km for a high F_{num} case.

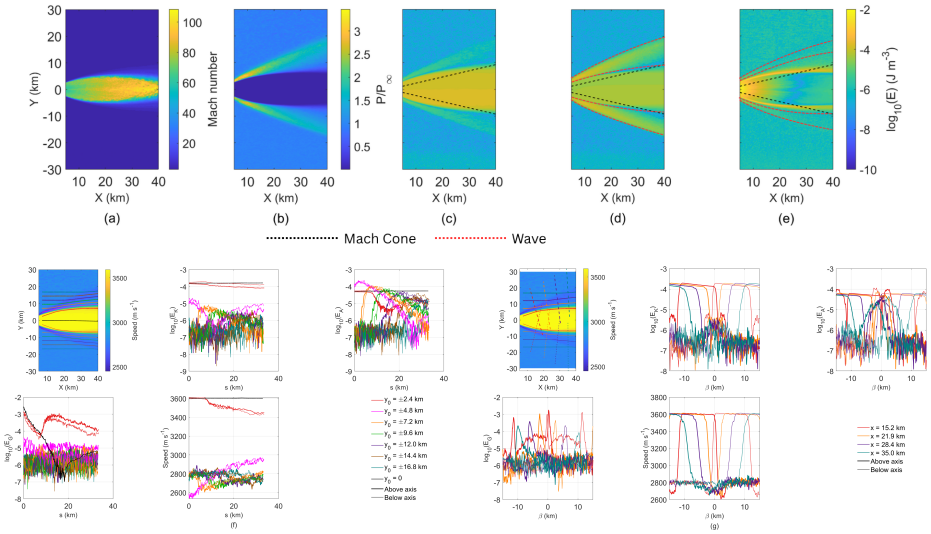


Fig. 5: 3D DSMC Case 2, 180 km case (XY Slice): (a) Mach number, (b) pressure ratio, (c) $\log_{10}(E_K)$, (d) $\log_{10}(E_A)$, and (e) $\log_{10}(E_G)$; (f) α along the streamline direction and (g) β perpendicular to the streamline direction.

7 Conclusions and Future Work

We have extended a previously reported 2D axisymmetric hybrid CFD/DSMC framework into a full 3D, gravitationally stratified pipeline, coupling the 2D CFD and 2D DSMC stages to a large-scale 3D DSMC stage via a converter applying NRLMSIS 2.0 stratification. A dual-resolution strategy was applied at 160 km and the high-F_{num} configuration at 180 km. The 3D results reproduce the shock and wave structures of the earlier 2D study but additionally show a marked upper/lower asymmetry attributable to the stratified thermosphere, with acoustic waves dominating over gravity waves through most of the domain. The agreement between the two F_{num} cases at 160 km supports using the larger, coarser domain for 180 km and for future larger domains.

Between 160 and 180 km, the shock structure and streamline trends are essentially unchanged, while the plume is longer and wider at 180 km. Acoustic energy remains prevalent at both altitudes, whereas gravity-wave energy is

weaker at 180 km and, already at 160 km, very weak relative to the acoustic response; it remains confined to the mixing region.

Future work includes analysing other trajectory points, a quantitative ground-based launch-identification measure from the wave features, larger domains to capture wave propagation and plume closure, comparison with TID observations [4, 8], non-Maxwellian distributions across interfaces, non-horizontal time-dependent trajectories, and ionosphere/plasma-chemistry coupling.

Acknowledgments. The authors gratefully acknowledge the University of New South Wales, Canberra, for providing computational resources. Data processing was performed on the computational facility of the National Computational Infrastructure (NCI) through the UNSW HPC Scheme (DOI: 10.26190/PMN5-7J50). The authors declare that this research received no external funding.

Disclosure of Interests. The authors have no competing interests to declare that are relevant to the content of this article.

References

1. Bird, G.A.: Molecular Gas Dynamics and the Direct Simulation of Gas Flows. Clarendon Press, Oxford (1994). https://doi.org/10.1093/oso/9780198561958.001.0001
2. Bowden, G.W., Lorrain, P., Brown, M.: Numerical simulation of ionospheric depletions resulting from rocket launches using a general circulation model. J. Geophys. Res. Space Physics **125**, e2020JA027836 (2020). https://doi.org/10.1029/2020JA027836
3. Bowden, G., Pollock, L., Brown, M.: Hybrid CFD/DSMC modelling of high-altitude rocket plumes. In: 24th Australasian Fluid Mechanics Conference, Canberra, Australia (2024). https://doi.org/10.5281/zenodo.14213606
4. Chou, M.-Y., Shen, M.-H., Lin, C.C.H., Yue, J., Chen, C.-H., Liu, J.-Y., Lin, J.-T.: Gigantic circular shock acoustic waves in the ionosphere triggered by the launch of FORMOSAT-5 satellite. Space Weather **16**(2), 172–184 (2018). https://doi.org/10.1002/2017SW001738
5. Emmert, J.T., et al.: NRLMSIS 2.0: A whole-atmosphere empirical model of temperature and neutral species densities. Earth Space Sci. **8**, e2020EA001321 (2021). https://doi.org/10.1029/2020EA001321
6. Gallis, M.A., Torczynski, J.R., Plimpton, S.J., Rader, D.J., Koehler, T.: Direct Simulation Monte Carlo: The quest for speed. In: 29th International Symposium on Rarefied Gas Dynamics, Xi'an, China (2014). https://doi.org/10.1063/1.4902571
7. Koura, K., Matsumoto, H.: Variable soft sphere molecular model for inverse-power-law or Lennard-Jones potential. Phys. Fluids A **3**(10), 2459–2465 (1991). https://doi.org/10.1063/1.858184
8. Lin, C.C.H., Shen, M.H., Chou, M.Y., Chen, C.H., Yue, J., Chen, P.C., Matsumura, M.: Concentric travelling ionospheric disturbances triggered by the launch of a SpaceX Falcon 9 rocket. Geophys. Res. Lett. **44**, 7578–7586 (2017). https://doi.org/10.1002/2017GL074192
9. Mendillo, M.: The effect of rocket launches on the ionosphere. Adv. Space Res. **1**(2), 275–290 (1981). https://doi.org/10.1016/0273-1177(81)90302-1
10. Yeh, K.C., Liu, C.H.: Acoustic-gravity waves in the upper atmosphere. Rev. Geophys. Space Phys. **12**(2), 193–216 (1974). https://doi.org/10.1029/RG012i002p00193